



Journal Name

COMMUNICATION

Geometric Modulation of Induced Plasmonic Circular Dichroism in Nanoparticle Assemblies Based on Backaction and Field Enhancement

Received 00th January 20xx,
Accepted 00th January 20xx

DOI: 10.1039/x0xx00000x

www.rsc.org/

Zhi Yong Bao,^{ab} Jiyan Dai,^a Qiang Zhang,^a Kwun Hei Ho,^a Siqi Li,^a Chan Cheuk Ho,^a Wei Zhang,^{c*}
Dang Yuan Lei^{*ad}

Chiral cysteine-directed assemblies of Au@Ag core-shell nanocrystals (CSNCs) and Au/Ag nanorods with end-to-end (ETE) and side-by-side (SBS) configurations are fabricated and used to explore the definitive factors affecting the chiral response. The interaction between the cysteine and metallic nanoparticles leads to intense and widely tunable plasmonic circular dichroism (PCD) ranged from near-infrared (NIR) to ultraviolet (UV) regime. More importantly, it was observed that, in Ag nanorod and CSNC samples with varied aspect ratio, the ETE assembled patterns exhibit much larger PCD enhancement than SBS assemblies in L/D-cysteine solvent environment. Very surprisingly, such a giant PCD response in these assemblies is completely different from that of the Au nanorod assembly case as reported earlier. Experimental and theoretical studies reveal that the interplay between the local field enhancement and backaction, triggered by the geometric configuration differentia of covered achiral CTAB molecules on Ag and Au surfaces, plays a crucial role in chiral response variances and leads to the geometry-dependent optical activities. This work not only sheds light on understanding the relationship between the configuration of plasmonic nanostructure assemblies and geometry-manipulated circular dichroism, but also paves the way for predictive design of plasmonic biosensors or other nanodevices with controllable optical activities from the UV to NIR light range.

Circular dichroism (CD), the differential absorption of left- and right-handed circularly polarized lights, is of particular importance in the chirality analyses of biomolecules.^{1,2} The CD spectroscopy can be used not only to unambiguously determine the enantiomer handedness, protein folding and conformational transition of chiral molecules,³⁻⁵ but also to elucidate the intrinsic relationship between

geometric structure and chiral response.⁶⁻¹⁴ Since the CD signals of those biomolecules like cysteine are located in the UV light region and typically weak,¹⁵⁻²⁵ it is vital to improve detection sensitivity for chiral analyses by extending/transferring the optical chirality from the UV region to the Vis-NIR range and increasing the chiral signal. Assembled nanoparticles can play an important role in tailoring the optical activity due to the tunability of nanostructures and the strong light-matter interaction in the designed systems.

Strong chiroptical effects have been reported from plasmonic nanoparticles assembled on the chiral scaffolds of organic fibers,¹⁸ or in nanoparticles that are assembled in chiral superstructures.¹⁹⁻²⁰ Such structures can also be elegantly assembled with the help of molecules, like DNA,²¹ and conversely, the plasmonic nanoparticles can enhance the chiroptical response of whole systems.²²⁻²³ Meanwhile, achiral nanoparticles (assemblies) have also been shown to exhibit strong chiroptical responses due to a near-field or long-range coupling through a layer of chiral molecules.²⁶⁻²⁷ In particular, strong PCD responses in hybrid nanostructures of achiral metal nanoparticles and chiral molecules, typically located at the plasmonic resonance bands, is accounted for the Coulomb interaction between the photo-induced transitions of molecules and metal nanoparticle electrons.²⁸⁻³¹ Because of the strong interplay between local electric and magnetic fields, these near-field electromagnetic coupling of dipoles and multipoles, as well as long-range radiating mechanisms significantly enhance the chiroptical effects. Currently, geometric modulation of chiral superstructures has been studied a lot.¹⁸⁻²⁵ While systematic exploring of molecule-induced chirality and the key factors affecting the induced PCD are lack, and need to be further studied because exploring the relationship between the configuration of nanostructure assemblies and geometry-manipulated CD is very important for predictive design of plasmonic biosensors or other nanodevices.

Experimental and theoretical studies reported on plasmon-enhanced CD spectroscopy with dissymmetry enhancement factors of up to 10⁵, which arises from plasmon-generated superchiral fields³²⁻³³ or near-field induced optical activity, both at isolated plasmonic nanostructures and at hotspots between closely spaced nanostructures.³⁴⁻³⁸ For instance, Kuang et al. demonstrated an

^a Department of Applied Physics, The Hong Kong Polytechnic University, Hong Kong. E-mail: dangyuan.lei@polyu.edu.hk

^b School of Materials Science and Engineering, Hefei University of Technology, Hefei, China

^c Institute of Applied Physics and Computational Mathematics, Beijing, China. E-mail: zhang_wei@iapcm.ac.cn

^d Shenzhen Research Institute, The Hong Kong Polytechnic University, Shenzhen, China

† Electronic Supplementary Information (ESI) available: Experimental details and additional figures and tables. See DOI: 10.1039/x0xx00000x

unusual circularly polarized photocatalytic activity in gold-gap-silver nanostructures with interior cysteine molecules.³⁵ Besides, rationally assembling plasmonic nanostructures is another effective means to achieve enhanced CD sensitivity.³⁹⁻⁴¹ In those assembled systems, one-dimensional assembly, which accommodates the propagation of squeezed light arising from near-field coupling between neighboring nanoparticles, is believed to achieve very strong electromagnetic enhancement and is promising in controlling the chiroptical properties because a proper modulation of optical activity at nanoscale is useful for exploring various mechanisms of PCD.⁴⁰

Au nanorods (NRs) assembled with collinear geometry could possess over two orders of magnitude of CD amplification for chiral molecules located at the hotspots.⁶ The distance between the chiral molecule and Au NR in the assembly unit was also demonstrated vital to the generated PCD signals.⁷ While Ag intrinsically possesses better plasmonic enhancement in comparison to other metallic nanoparticles, Au featured with excellent stability can serve as an inner core template for coating with Ag shells.^{26,40} For instance, the CD signal of a novel chiroptical biosensor based on aptamer-mediated Au NR dimers could be further amplified by depositing Ag shells on metallic nanoparticles) determines the induced PCD of the CSNC assemblies, which is different from previous studies.⁴⁵⁻⁴⁸

be tailored by changing the building blocks, geometrical parameters, interparticle distances, orientational arrangements.^{43,44} However, to date understanding and manipulating the PCD responses of Au@Ag CSNC assemblies remains a considerable challenge due to the multiple mechanisms involved and the restriction of precisely controlled structure geometry, interparticle distance as well as mutual orientation between CSNCs in the assemblies. Therefore, it is pressing to explore various factors that influence the optical activity based on a reliable model system of CSNC assemblies.

Here we investigate the chiroptical response of cysteine-directed self-assembly of CSNCs within SBS and ETE patterns. The PCD response of the resultant hybrid nanostructures is found highly dependent on the geometry of the assembly patterns and the electromagnetic interaction between neighboring CSNCs. Nevertheless, using the self-assembly method, well-defined patterns of CSNC could be achieved, thereby offering the possibility to explore the key factors of the geometry-dependent PCD. Our experimental and theoretical studies reveal that the interplay between the geometry-dependent local field enhancement (at the hot spots due to metallic nanoparticles) and backaction (of cysteine

Fig. 1a presents a typical assembly case of Au@Ag CSNC with an average aspect ratio of ~ 3.8 , demonstrating the distinct

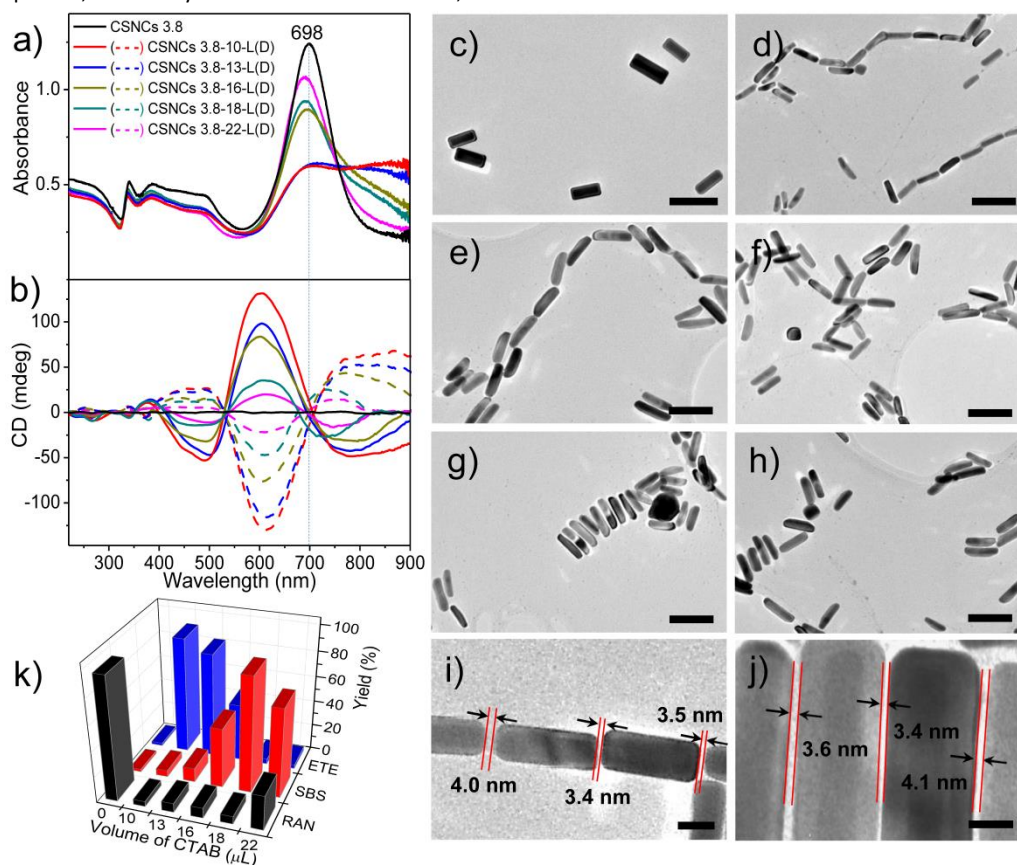


Fig. 1 (a, b) Absorption and CD spectra of pristine CSNCs and L/D-cysteine assembled CSNCs under different CTAB concentrations. Representative TEM images of (c) pristine CSNCs and the L-cysteine assembled CSNCs under different CTAB concentrations: (d)10, (e)13, (f)16, (g)18, (h)22 μM . The scale bar is 100 nm. Here the CSNCs have an aspect ratio of 3.8. (i, j) Magnified TEM images of ETE and SBS patterns, respectively. The interparticle distances between adjacent CSNCs have been measured; the scale bar are 15 nm (i) and 10 nm (j), respectively. (k) Statistic distributions of different assembly patterns of L-cysteine-CSNCs formed under varied CTAB concentration. "RAN" represents random arrangement.

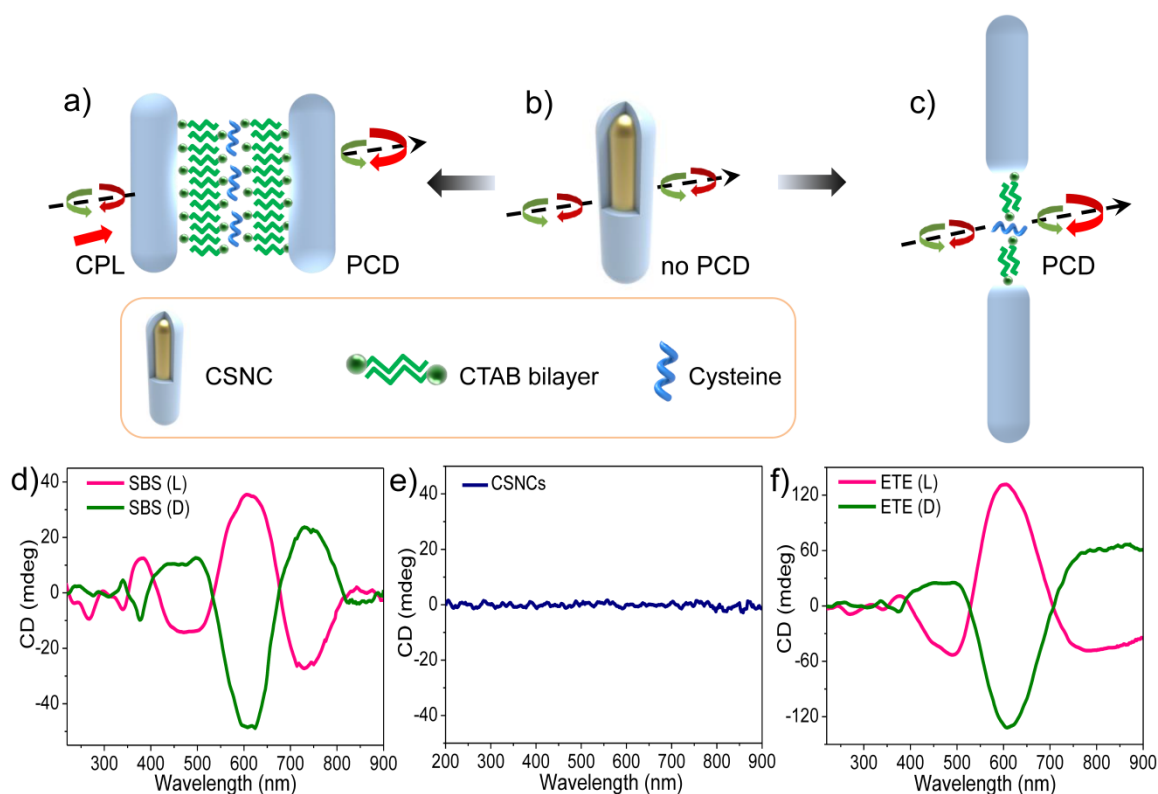


Fig. 2 Diagrams of pristine Au@Ag CSNCs (b) and cysteine-assembled CSNCs in SBS (a) and ETE (c) patterns. (d-f) are corresponding CD spectra for SBS assembly (d), pristine CSNCs (e) and ETE assembly (f), respectively.

assembly behavior under varied concentration of CTAB (the absorption spectra of D-cysteine assembled samples are shown in Fig. S1). At a low CTAB concentration of 10 μM (red curve), the intensity of the longitudinal LSP absorption peak is sharply reduced upon addition of cysteine, whereas a new absorption shoulder appears in the 800–900 nm region. These are the typical characteristics of the ETE assembly.⁴⁹ When the concentration of CTAB increases to 18 μM (cyan curve), addition of cysteine results in both intensity decrease and blueshift of the LSP absorption peak (from 698 nm to 683 nm), which is a feature of SBS assembled CSNCs. The calculated absorption cross sections of single Au@Ag CSNC (Fig. S2), ETE and SBS assembled samples (Fig. S3) match well with the experimental results. Note that a small amount of CSNCs assembled with ETE geometry may still exist, which leads to the shoulder in the red wavelength region and small correction to the chiral response. As the CTAB concentration further increases, the intensity of the LSPR peak is instead increased, and the peak position redshifts, implying the SBS assembly patterns reduced. It was found that, with no cysteine, the LSPRs of CSNCs at various concentrations of CTAB are similar but a little red-shift with the increase of CTAB (see Fig S4). Straightforward observation by TEM imaging further proves the assembly transition of CSNC from ETE to SBS pattern (Fig. 1d–1h). Fig. 1i and 1j show the measured interparticle distances between adjacent CSNCs in both ETE and SBS assemblies are ~ 3 –5 nm. The corresponding statistical analysis (Fig. 1k) confirms the transition of CSNC assemblies from ETE to SBS dominated mode (more TEM images are shown in Fig. S5).

The CD spectra of L-cysteine assembled CSNCs (solid curves) in Fig. 1b, reveal that both ETE and SBS modes possess four CD peaks

near the frequency of LSP absorption bands, while the former shows much higher CD enhancement than the latter overall. The large PCD amplification of the ETE CSNCs is originated mostly from the strong electromagnetic field at the hotspots located in the gaps between Ag ends. Surface-enhanced Raman spectroscopy (SERS) further provides the near-field information at hot spots of noble metal nanoparticles.⁵⁰ Hence, the SERS spectra of both ETE and SBS assemblies were recorded for comparing the electromagnetic effect, and the intensity of C–S stretching vibration of L-cysteine molecules was chosen as a standard. Obviously, the SERS intensity of ETE assembled CSNCs is much higher than that in the SBS pattern (Fig. S6). The CD peaks located at 383 and 334 nm correspond to octupolar and multipole LSP modes, while the low energy peaks 497 and 698 nm are attributed to the transverse and longitudinal dipolar LSPR, respectively (Fig. S2 and S3). The induced PCD is due to the Coulomb interaction (see the theoretical details) instead of the twist of CSNC pairs, which is supported by the fact that in the racemic DL-cysteine assembled CSNCs, neither the ETE nor the SBS assembly pattern show detectable CD response (Fig. S7). The proposed mechanism is further verified by the chiroptical response of D-cysteine assembled CSNCs, in which the PCD displays a mirror symmetry feature as the L-cysteine assembled systems (see dashed curves in Fig. 1b). The D-cysteine assembled nanostructures exhibit the same geometry-manipulated PCD response with the variation of CTAB concentration. The detailed PCD signal comparison between L- and D-cysteine-constructed typical assemblies is shown as following.

At a low concentration of CTAB, a considerable amount of cysteine molecules will adsorb at the CSNC end positions with high

bonding energies, thereby leading to the formation of ETE assemblies (Fig. 2c). On the contrary, at a high concentration the number of CTAB surfactants is sufficient to stabilize the whole assembly behavior under varied concentration of CTAB (the absorption spectra of D-cysteine assembled samples are shown in Fig. S1). At a low CTAB concentration of 10 μM (red curve), the intensity of the longitudinal LSP absorption peak is sharply reduced upon addition of cysteine, whereas a new absorption shoulder appears in the 800–900 nm region. These are the typical characteristics of the ETE assembly.⁴⁹ When the concentration of CTAB increases to 18 μM (cyan curve), addition of cysteine results in both intensity decrease and blueshift of the LSP absorption peak (from 698 nm to 683 nm), which is a feature of SBS assembled CSNCs. The calculated absorption cross sections of single Au@Ag CSNC (Fig. S2), ETE and SBS assembled samples (Fig. S3) match well with the experimental results. Note that a small amount of CSNCs assembled with ETE geometry may still exist, which leads to the shoulder in the red wavelength region and small correction to the chiral response. As the CTAB concentration further increases, the intensity of the LSPR peak is instead increased, and the peak position redshifts, implying the SBS assembly patterns reduced. Straightforward observation by TEM imaging further proves the assembly transition of CSNC from ETE to SBS pattern (Fig. 1d–1h). Fig. 1i and 1j show the measured interparticle distances between adjacent CSNCs in both ETE and SBS assemblies are ~ 3 –5 nm.

The CD spectra of L-cysteine assembled CSNCs (solid curves) in Fig. 1b, reveal that both ETE and SBS modes possess four CD peaks near the frequency of LSP absorption bands, while the former shows much higher CD enhancement than the latter overall. The large PCD amplification of the ETE CSNCs is originated mostly from the strong electromagnetic field at the hotspots located in the gaps between Ag ends. Surface-enhanced Raman spectroscopy (SERS) further provides the near-field information at hot spots of noble metal nanoparticles.⁵⁰ Hence, the SERS spectra of both ETE and SBS assemblies were recorded for comparing the electromagnetic effect, and the intensity of C–S stretching vibration of L-cysteine molecules was chosen as a standard. Obviously, the SERS intensity of ETE assembled CSNCs is much higher than that in the SBS pattern (Fig. S6). The CD peaks located at 383 and 334 nm correspond to octupolar and multipole LSP modes, while the low energy peaks 497 and 698 nm are attributed to the transverse and longitudinal dipolar LSPR, respectively (Fig. S2 and S3). The induced PCD is due to the Coulomb interaction (see the theoretical details) instead of the twist of CSNC pairs, which is supported by the fact that in the racemic DL-cysteine assembled CSNCs, neither the ETE nor the SBS assembly pattern show detectable CD response (Fig. S7). The proposed mechanism is further verified by the chiroptical response of D-cysteine assembled CSNCs, in which the PCD displays a mirror symmetry feature as the L-cysteine assembled systems (see dashed curves in Fig. 1b). The D-cysteine assembled nanostructures exhibit the same geometry-manipulated PCD response with the variation of CTAB concentration. The time-dependent LSP and CD spectra changes are also recorded (details are shown in Fig. S8). The detailed PCD signal comparison between L- and D-cysteine-constructed typical assemblies is shown as following.

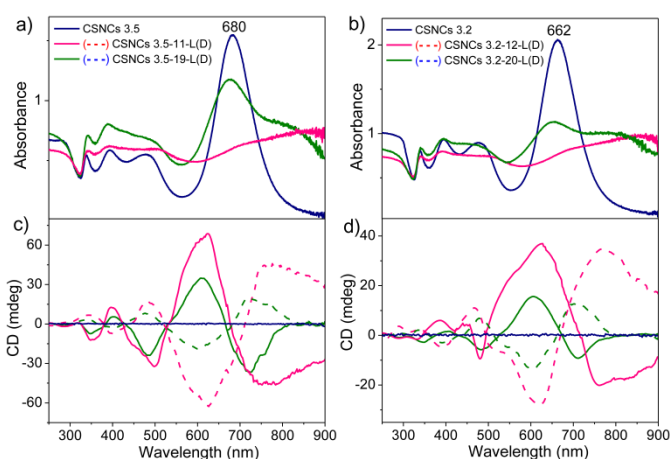


Fig. 3 Comparison of absorption and CD spectra of ETE (pink curves) and SBS (green curves) assembled CSNCs with aspect ratio of (a, c) ~ 3.5 and (b, d) ~ 3.2 . The numbers 11, 12, 19 and 20 in the labels represent the concentration of CTAB used in the experiment.

At a low concentration of CTAB, a considerable amount of cysteine molecules will adsorb at the CSNC end positions with high bonding energies, thereby leading to the formation of ETE assemblies (Fig. 2c). On the contrary, at a high concentration the number of CTAB surfactants is sufficient to stabilize the whole surface of CSNCs, eliminating the energy difference between the sides and ends toward adsorption of cysteine molecules. In this case, SBS assemblies tend to form due to the larger surface area of the sides compared with that of the ends (Fig. 2a). The assembly patterns have important impact on the chiroptical responses of the hybrid nanostructures. Fig. 2b and 2e show that pristine CSNCs have no CD response. Although the ETE and SBS assemblies experience giant PCD responses with similar line shape as shown in Fig. 2d and 2f, the former shows superior performance in PCD sensitivity. In general, the g factor of a positive or negative CD peak corresponding to the longitudinal LSPR is used for quantitative comparison of PCD sensitivity. As can be seen from Table S1, the g-factors for L and D-cysteine constructed ETE patterns are 1.6 and 1.8 times (14.45×10^{-3} vs 8.97×10^{-3} and 11.7×10^{-3} vs 6.43×10^{-3}) larger than their SBS counterparts, respectively. Noted that insufficient (e.g. 1 μM) or excess CTAB (e.g. 200 μM) in the solution could not induce distinct PCD signals (details are shown in Fig. S9).

In order to further elaborate the generality of the observed geometry-modulated chiroptical responses, L/D-cysteine molecules were successfully employed to assemble Au@Ag CSNCs with different aspect ratios under the control of CTAB surfactant concentration (see TEM images in Fig. S10). The measured PCD spectra are shown in Fig. 3. With the CSNCs aspect ratio decreases, the bisignated CD bands show a spectral blueshift, due to the corresponding blueshift of the longitudinal LSPR. Meanwhile, the PCD signal intensities of ETE and SBS assembled CSNCs decrease accordingly due to the decreasing backaction of cysteine on CSNCs (see the theoretical analysis). It is interesting to observe that, in all the samples with different aspect ratios, the ETE assembled CSNCs presented much more PCD enhancement than the SBS assemblies either in L-cysteine or D-cysteine solvent environment (Table S2 and S3). Very surprisingly, such a rich PCD response in CSNC assemblies

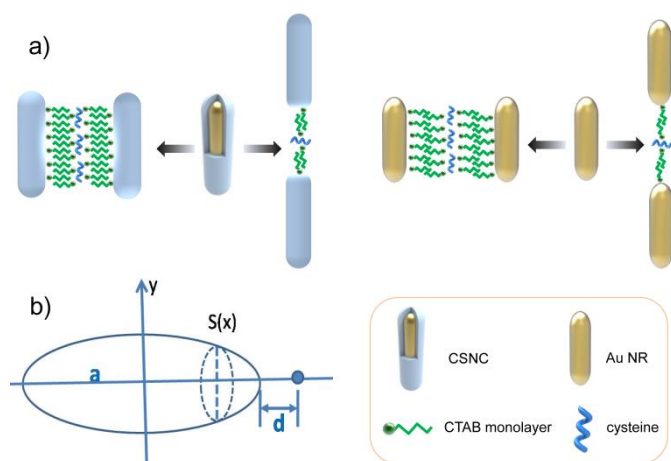


Fig. 4 (a) Proposed molecular arrangement difference of capped CTAB on the surface of Ag and Au. (b) The constructed model used in theoretical calculations.

is different from that of Au NR assembly case as we reported earlier.⁷ Here, control experiments of cysteine-assembled Au NRs in both ETE and SBS patterns were also performed under similar experimental conditions. It's apparent that the CD enhancement of SBS assembled Au NRs is much higher than ETE assembled ones (0.86×10^{-3} vs 0.55×10^{-3} , Fig. S11). Such different responses of PCD are unexpected, and it has motivated us to explore an intrinsic relationship between geometric configuration and PCD response in cysteine-assembled Au@Ag CSNCs/Au/Ag NRs, which have been overlooked in previous studies.^{7,51}

Basically, it is difficult to prove or disprove that the chiral molecules influence the assembly of the nanostructures.⁵² Nevertheless, it is reported that supported CTAB surfactants with long flexible hydrophobic tails and positively charged hydrophilic head groups can act as protecting agent, and structure-directing agent that are involved in the formation of anisotropic nanostructures of Au or Ag. The molecular configuration of CTAB adsorbed on Au or Ag nanoparticle surface has been extensively investigated. Previous studies involved small-angle X-ray scattering, TEM imaging and molecular dynamics simulations show that the thickness of CTAB decorated on the surface of Au nanoparticles is ~ 3 nm⁵³ while the length of a CTAB molecular monolayer is ~ 1.5 nm.⁵⁴ Thus, an uncommon interdigitated bilayer CTAB nanostructure adsorbed on Au NRs was felicitously proposed and this proposal was further verified in our recent work,⁷ which is different from that molecular arrangement of capped CTAB on the surface of Ag (Fig. 4 and Fig. S12). Previous experimental and calculation studies revealed that CTA⁺ chains display a considerable degree of curvature when CTAB molecules form bilayer on Ag surface.⁵⁵⁻⁵⁷ It means that CTAB molecules either in inner or outer layers do not pack in a full-extended state but bend or twist to each other, which could result in a much smaller thickness of adsorbed layer than twice length of CTAB molecules.⁵⁷ In our work, TEM imaging in Fig. 1i and 1j discloses the gap distance between assembled adjacent CSNCs is ~ 3.5 -4 nm, further demonstrates the curved CTAB orientation coated on the Ag surface. These structural characteristics provide new insights for better understanding the geometry-correlated chiroptical properties. Besides the material

difference of Au and Ag (which leads to different characters of field concentration), they may lead to different gap sizes, which is essential for both the local field enhancement and backaction of cysteine on CSNCs (see the theoretical analysis). Within this nano-sized gap the incident light is squeezed in the hotspot and hence the geometry-modulated optical activity could be greatly enhanced.

To elaborate the arrangement difference of capped CTAB molecules upon adsorption on Ag and Au, we performed additional proof experiment in which cysteine was selected to assemble Ag NRs. Again, the g-factor of ETE assembled Ag NRs is much higher than its SBS counterpart (1.11×10^{-3} vs 0.32×10^{-3} , Fig. S13). Therefore, the configuration difference of covered achiral CTAB between on Au and Ag surface is very important for PCD enhancement mechanisms. Within a much smaller distance between Ag ends compared with the Au-Au gap for Au assemblies, the gigantic electric field located at the hotspots between coupled adjacent CSNCs will determine the induced PCD response. In fact, gap-plasmonic nano-antennas can enhance the coupling between free-space propagating light and the localized excitation of nanoscopic light emitters or receivers, thus forming the optical basis of many gap-dependence nanophotonic applications.⁵⁸⁻⁶⁰ For example, the distance dependence of near-field fluorescence enhancement and quenching of single quantum dots has been demonstrated by Walhorn.⁵⁸ A distance-dependent plasmon resonant coupling between Au NP and Au film was presented by Mock and co-workers.⁵⁹ Parak et al. reported that the studies about electromagnetic coupling were highly dependent on controlled interparticle distance between adjacent plasmonic nanoparticles.⁶⁰

In order to further comprehend the relationship between geometric configuration and PCD response, we performed systematic theoretical investigation. The Coulomb interaction between the photo-induced excitation of molecules and plasmon of metal nanoparticle plays the key role in PCD. We develop a theory of cysteine-induced PCD to reveal the main factors affecting the chiral response of the hybrid nanostructures. In our model shown in Fig. 4b, we consider core-shell nanocrystal assemblies (with ETE or SBS configuration) incorporating the dipole of CYS (cysteine) at the centre of the gaps. The dominant contribution of CD comes from CYS-induced PCD. The CD signal of the nanocrystals is given by the difference of optical absorption (Q_{CSNC}^L) between the left/right circularly polarized fields, that is, $\text{CD}_{\text{CSNC}} = Q_{\text{CSNC}}^L - Q_{\text{CSNC}}^R$ with

$$Q_{\text{CSNC}}^R \propto \int dV \left(\vec{E}_0 + \vec{E}_D^R \right) \cdot \left(\vec{E}_0 + \vec{E}_D^L \right) \quad (1)$$

$$\vec{E}_D^{L/R}(r, r_D) = G(r, r_D) p_D^{L/R}(r_D) \quad (2)$$

where \vec{E}_0 is the incident field and $\vec{E}_D^{L/R}$ is the induced field due to CYS, $\vec{E}_0 + \vec{E}_D^{L/R}$ is the local field on the nanocrystal, $G(r, r_D)$ (r and r_D are the coordinate centers of the CSNC and cysteine) reflects the distance dependence of the backaction of cysteine on the CSNC. In Equation (2), $p_D^{L/R}$ is the effective dipole moment of CYS (at r_D) for the left/right circularly polarized fields,

$$p_D^{L/R} = \alpha^{L/R} E_C n_{\text{CYS}} \quad (3)$$

where E_C is the local field on CYS, and n_{CYS} is the number of CYS molecules adsorbed in the gap. The chirality of the molecules

comes from the electric dipole moment and the magnetic dipole moments. One can have the effective dipole moment $p_D^{L/R}$ determined by the effective polarizabilities $\alpha^{L/R}$ (including the effects from both moments) for the left/right circularly polarized fields.⁶¹⁻⁶² We therefore obtain the following equation:

$$CD_{CSNC} = A \cdot n_{CYS} \cdot \text{Re}(\int \Delta\alpha \cdot E_0^* \cdot E_C \cdot G(r, r_D) dV) \quad (4)$$

where $\Delta\alpha = \alpha^L - \alpha^R$, and A is a constant. For the ETE configuration, we can calculate the CD_{CSNC} approximately as follows:

$$CD_{CSNC} \sim n_{CYS} \cdot \Delta\alpha \cdot E_C \cdot \int \frac{S(x)}{r^3} dx, \quad (5)$$

where $S(x)$ is the area at position x , and $r = |a+d-x|$. For the case of large $a+d$, we have $G(r, r_D) \propto 1/|a+d-x|^3$. Similar calculation can be applied to the SBS configuration. The anisotropic factor can be obtained as $g = CD_{CSNC}/Abs_{CSNC} \propto E_C \cdot [\int S(x)/r^3 dx]/Abs_{CSNC}$, where Abs_{CSNC} refers to the absorption coefficient of the core-shell nanocrystal. In the calculation, we have used the discrete dipole approximation (DDA)⁶³⁻⁶⁴ method to obtain E_C and Abs_{CSNC} . We can theoretically calculate the enhancement factor for the ETE mode against the SBS mode based on above formulism. For instance, enhancement factors (i.e., g_{ETE}/g_{SBS}) at the longitudinal LSP resonance bands are 1.37, 3.39, and 3.80 for CSNCs with aspect ratio of 3.8, 3.5, and 3.2, respectively.

For comparison, we also calculate the g-factors of Ag/Au NR assemblies based on the same formulism and the g-factor ratios g_{ETE}/g_{SBS} at their longitudinal LSP resonance bands are 3.31 for Ag NR assemblies (experiment: 3.47), 0.69 for Au NR assemblies (experimental result: 0.64). Our theoretical results agree well with the experimental observations. Moreover, our theory reveals the main factors affecting the chiral response for hybrid nanostructures with different geometric configurations and may suggest new methods for the geometric manipulation of induced PCD responses. From equation (4), we can see that the PCD is proportional to $\Delta\alpha$, indicating the PCD signal is induced by the cysteine. Furthermore, the PCD is proportional to E_C (gap field at the hotspots due to the metallic nanoparticles) and $G(r, r_D)$ (backaction of CYS on the metallic nanoparticles). In general, with decreasing the gap distance (2d), both $G(r, r_D)$ and the gap field E_C increase. The combination of these two gap distance dependent factors determines the geometric dependence of the chiral response. For the Au@Ag and Ag assemblies with small gap distance (2d), Ag leads to strong field concentration, i.e., E_C in the ETE configuration, resulting in larger enhancement factor, $g_{ETE}/g_{SBS} > 1$. While in the case of Au NR assemblies, the gap distance is larger than that in the Au@Ag and Ag assemblies, and therefore the $G(r, r_D)$ plays a more important role, which leads to $g_{ETE}/g_{SBS} < 1.7$. In general, the PCD response of Au, Ag, Au@Ag CSNC assemblies is the combined contribution from both the electromagnetic field effect at the hotspots and the geometry-dependent electromagnetic backaction. Thus, different geometric configurations (ETE & SBS) lead to different electromagnetic fields at hotspots and backaction amplitudes, which brings about interesting geometry-dependent chiral characteristics for Au@Ag CSNC, Ag and Au NR assemblies.

Conclusions

In summary, Au@Ag CSNC/Ag NR/Au NR assemblies have been successfully constructed by cysteine in two representative ETE and SBS patterns to explore the crucial factors affecting their chiral responses. Manipulation of the Ag shell thickness coated on Au NR enables spectral modulation of their chiroplasmonic bands from the NIR to UV light region and results in significantly enhanced chiroptical responses with a maximal g-factor reaching $\sim 14.45 \times 10^{-3}$, where the strong near-field at the hotspots is responsible for the PCD improvement. More interestingly, we observe that ETE assembled CSNCs/Ag NRs with cysteine present larger PCD response than the SBS assemblies, which is different from that of the Au NR assembly case. Experimental and theoretical demonstration reveals that the interplay between the local field enhancement and backaction due to the geometric configuration differentia of covered achiral CTAB molecules adsorbed on Ag/Au surface dominates the different PCD enhancement mechanisms. This work lays the foundation to explore tunable and intense PCD responses via construction of designed surfactant-caped building blocks, which holds great potential for chiral sensing, biomedicine and optoelectronic devices.

Conflicts of interest

There are no conflicts to declare.

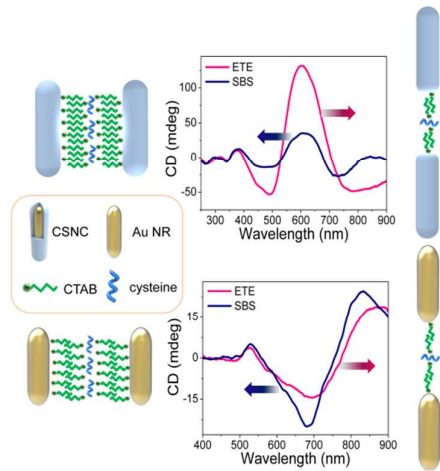
Acknowledgements

The authors acknowledge the National Key Research and Development Program of China (Grant Nos. 2017YFA0303400, 2013CB632805), the National Natural Science Foundation of China (Grant Nos. 51802066, 11474240, 11774036, 11374039), and The Hong Kong Polytechnic University (1-ZE23). Z. Y. Bao and J. Dai contributed equally to this work.

References

- 1 Y. Wang, J. Xu., Y. Wang, H. Chen, *Chem. Soc. Rev.*, 2013, **42**, 2930.
- 2 A. Kuzyk, R. Schreiber, H. Zhang, A. O. Govorov, T. Lied and N. Liu, *Nat. Mater.*, 2014, **13**, 862.
- 3 B. M. Maoz, R. Weegen, Z. Fan, A. O. Govorov, G. Ellestad, N. Berova, E. W. Meijer, and G. Markovich, *J. Am. Chem. Soc.*, 2012, **134**, 17807.
- 4 I. Lieberman, G. Shemer, T. Fried, E. M. Kosower, and G. Markovich G., *Angew. Chem. Int. Ed.*, 2008, **47**, 4855.
- 5 Z. Y. Bao, W. Zhang, Y.-L. Zhang, J. He, J. Dai, C.-T. Yeung, G.-L. Law, and D. Y. Lei, *Angew. Chem. Int. Ed.*, 2017, **56**, 1283.
- 6 Z. N. Zhu, W. J. Liu, Z. T. Li, B. Han, Y. L. Zhou, Y. Gao, Z. Y. Tang, *ACS Nano*, 2012, **6**, 2326.
- 7 B. Han, Z. Zhu, Z. Li, W. Zhang, Z. Y. Tang, *J. Am. Chem. Soc.*, 2014, **136**, 16104.
- 8 D. Zhai, P. Wang, R.-Y. Wang, X. Tian, Y. Ji, W. Zhao, L. Wang, H. Wei, X. Wu, X. Zhang, *Nanoscale*, 2015, **7**, 10690.
- 9 M. Kuwata-Gonokami, N. Saito, Y. Ino, M. Kauranen, K. Jefimovs, T. Vallius, J. Turunen, Y. Svirko, *Phys. Rev. Lett.*, 2005, **95**, 227401(1-4).
- 10 V. K. Valev, N. Smisdom, A. V. Silhanek, B. De Clercq, W. Gillijns, M. Ameloot, V. V. Moshchalkov, T. Verbiest, *Nano Lett.*, 2009, **9**, 3945.

- 11 J. K. Gansel, M. Thiel, M. S. Rill, M. Decker, K. Bade, V. Saile, G. von Freymann, S. Linden, M. Wegener, *Science*, 2009, **325**, 1513.
- 12 M. Decker, M. Ruther, C. E. Krieglger, J. Zhou, C. M. Soukoulis, S. Linden, M. Wegener, *Opt. Lett.*, 2009, **34**, 2501.
- 13 N. Liu, H. Liu, S. Zhu, H. Giessen, *Nat. Phot.*, 2009, **3**, 157.
- 14 V. K. Valev, J. J. Baumberg, C. Sibilia, and T. Verbiest, *Adv. Mater.*, 2013, **25**, 2517.
- 15 C. Shen, X. Lan, X. Lu, W. Ni and Q. Wang, *Chem. Commun.*, 2015, **51**, 13627
- 16 X. Wu, L. Xu, L. Liu, W. Ma, H. Yin, H. Kuang, L. Wang, C. Xu, N. A. Nicholas, *J. Am. Chem. Soc.*, 2013, **135**, 18629.
- 17 H. Zhang and A. O. Govorov, *Phys. Rev. B*, 2013, **87**, 075410(1-8).
- 18 A. Guerrero-Martinez, B. Augu  , J. Lorenzo Alonso-Gomez, Z. Dzolic, S. Gomez-Grana, M. Zinic, M. Magdalena Cid, L. M. Liz-Marzan, *Angew. Chem. Int. Ed.*, 2011, **50**, 5499.
- 19 M. Hentschel, M. Schaferling, T. Weiss, N. Liu, H. Giessen, *Nano Lett.*, 2012, **12**, 2542.
- 20 Z. Fan, A. O. Govorov, *Nano Lett.*, 2010, **10**, 2580.
- 21 A. J. Mastroianni, S. A. Claridge, A. Paul Alivisatos, *J. Am. Chem. Soc.*, 2009, **131**, 8455.
- 22 A. O. Govorov, *J. Phys. Chem. C*, 2011, **115**, 7914.
- 23 A. O. Govorov, Z. Fan, P. Hernandez, J. M. Slocik, R. R. Naik, *Nano Lett.*, 2010, **10**, 1374.
- 24 C. Shen, X. Lan, C. Zhu, W. Zhang, L. Wang, and Q. Wang, *Adv. Mater.*, 2017, **29**, 1606533(1-8).
- 25 W. Zhang, *Chirality at Nanoscale-Theory and Mechanism in Chiral Nanomaterials: Preparation, Properties and Applications*, Z. Y. Tang, John Wiley & Sons, Inc., 2018.
- 26 A. Kuzyk, R. Schreiber, Z. Fan, G. Pardatscher, E.-M. Roller, A. H  gele, F. C. Simmel, A. O. Govorov and T. Liedl, *Nature*, 2012, **483**, 311.
- 27 Y. Zhou, Z. Zhu, W. Huang, W. Liu, S. Wu, X. Liu, Y. Gao, W. Zhang and Z. Tang, *Angew. Chem. Int. Ed.*, 2011, **50**, 11456.
- 28 W. Zhang, A. O. Govorov, G. W. Bryant, *Phys. Rev. Lett.*, 2006, **97**, 146804(1-4).
- 29 S. H. Jung, J. Jeon, H. Kim, J. H. Jung, *J. Am. Chem. Soc.*, 2014, **136**, 6446.
- 30 C. Song, M. G. Blaber, G. Zhao, P. Zhang, H. C. Fry, G. C. Schatz, N. L. Rosi, *Nano Lett.*, 2013, **13**, 3256.
- 31 W. Liu, Z. Zhu, K. Deng, S. Li, Y. Zhou, H. Qiu, Y. Gao, S. Chen, Z. Tang, *J. Am. Chem. Soc.*, 2013, **135**, 9659.
- 32 M. L. Nesterov, X. Yin, M. Sch  ferling, H. Giessen and T. Weiss, *ACS Photonics*, 2016, **3**(4), 578.
- 33 Y. Tang, A. E. Cohen, *Science*, 2011, **332**, 333.
- 34 N. A. Abdulrahman, Z. Fan, T. Tonooka, S. M. Kelly, N. Gadegaard, E. Hendry, A. O. Govorov, M. Kadodwala, *Nano Lett.*, 2012, **12**, 977.
- 35 B. M. Maoz, R. van der Weegen, Z. Fan, A. O. Govorov, G. Ellestad, N. Berova, E. W. Meijer, G. Markovich, *J. Am. Chem. Soc.*, 2012, **134**, 17807.
- 36 F. Lu, Y. Tian, M. Liu, D. Su, H. Zhang, A. O. Govorov, O. Gang, *Nano Lett.*, 2013, **13**, 3145.
- 37 C. Hao, L. Xu, W. Ma, X. Wu, L. Wang, H. Kuang and C. Xu, *Adv. Funct. Mater.*, 2015, **25**, 5816.
- 38 X. Wu, L. Xu, W. Ma, L. Liu, H. Kuang, W. Yan, L. Wang and C. Xu, *Adv. Funct. Mater.*, 2015, **25**, 850.
- 39 L. Xu, Z. Xu, W. Ma, L. Liu, L. Wang, H. Kuang and C. Xu, *J. Mater. Chem. B*, 2013, **1**, 4478.
- 40 X. Shen, P. Zhan, A. Kuzyk, Q. Liu, A. Asenjo-Garcia, H. Zhang, F. Javier Garc  a de Abajo, A. Govorov, B. Dingand N. Liu, *Nanoscale*, 2014, **6**, 2077.
- 41 W. Ma, H. Kuang, L. Xu, L. Ding, C. Xu, L. Wang and N. A. Kotov, *Nat. Commun.*, 2013, **4**, 2689(1-8), DOI:10.1038/ncomms3689.
- 42 L. Tang, S. Li, L. Xu, W. Ma, H. Kuang, L. Wang and C. Xu, *ACS Appl. Mater. Interfaces*, 2015, **7**, 12708.
- 43 Y. Zhao, L. Xu, W. Ma, L. Wang, H. Kuang, C. Xu and N. A. Kotov, *Nano Lett.*, 2014, **14**, 3908.
- 44 Z. Zhu, J. Guo, W. Liu, Z. Li, B. Han, W. Zhang, Z. Tang, *Angew. Chem. Int. Ed.*, 2013, **52**, 13571.
- 45 C. Hao, L. Xu, W. Ma, L. Wang, H. Kuang, C. Xu, *Small*, 2014, **10**, 1805.
- 46 C. Hao, L. Xu, M. Sun, W. Ma, H. Kuang, C. Xu, *Adv. Funct. Mater.*, 2018, **28**, 1802372.
- 47 X. Zhao, L. Xu, M. Sun, W. Ma, X. Wu, C. Xu, H. Kuang, *Nat. Commun.*, 2017, **8**, 2007.
- 48 M. Sun, L. Xu, J. Bahng, H. Kuang, S. Alben, N. A. Kotov, C. Xu, *Nat. Commun.* 2017, **8**, 1847.
- 49 P. K. Jain, S. Eustis, M. A. El-Sayed, *J. Phys. Chem. B*, 2006, **110**, 18243.
- 50 Z. Y. Bao, D. Y. Lei, R. Jiang, X. Liu, J. Dai, J. Wang, L. W. C. Helen, Y. H. Tsang, *Nanoscale*, 2014, **6**, 9063.
- 51 A. Lee, G. F. S. Andrade, A. Ahmed, M. L. Souza, N. Coombs, E. Tumarkin, K. Liu, R. Gordon, A. G. Brolo, E. Kumacheva, *J. Am. Chem. Soc.*, 2011, **133**, 7563.
- 52 S. Hou, H. Zhang, J. Yan, Y. Ji, T. Wen, W. Liu, Z. Hu and X. Wu, *Phys. Chem. Chem. Phys.*, 2015, **17**, 8187.
- 53 A. M. Alkilany, R. L. Frey, J. L. Ferry, C. J. Murphy, *Langmuir*, 2008, **24**, 10235.
- 54 R. M. Pashley, P. M. McGuiggan, R. G. Horn, B. W. Ninham, *J Colloid Interface Sci.*, 1988, **126**, 569.
- 55 Z. M. Sui, X. Chen, L. Y. Wang, L. M. Xu, W. C. Zhuang, Y. C. Chai, C. J. Yang, *Physica E*, 2006, **33**, 308.
- 56 C. Yang, X. Chen, Z. Sui, L. Wang, *Colloids Surf. A*, 2006, **274**, 219.
- 57 Z. Khan, J. I. Hussain, A. A. Hashmi, S. A. AL-Thabaiti, *Arab. J. Chem.*, 2017, **10**, S1506.
- 58 V. Walhorn, J. Paskarkeit, H. G. Frey, A. Harderand D. Anselmetti, *Beilstein J. Nanotechnol.*, 2011, **2**, 645.
- 59 J. J. Mock, R. T. Hill, A. Degiron, S. Zauscher, A. Chilkoti and D. R. Smith, *Nano Lett.*, 2008, **8**, 2245.
- 60 X. Yu, D. Y. Lei, F. Amin, R. Hartmann, G. P. Acuna, A. Guerrero-Mart  nez, S. A. Maier, P. Tinnefeld, S. Carregal-Romero, W. J. Parak, *Nano Today*, 2013, **8**, 480.
- 61 Fasman, G. D. (Editor), *Circular dichroism and the conformational analysis of biomolecules*, Plenum: New York, USA 1996.
- 62 P. Fischer and F.Hache, *Chirality*, 2005, **17**, 421.
- 63 B. T. Draine, *Astrophys. J.*, 1988, **333**, 848.
- 64 B. T. Draine and P. J. Flatau, *J. Opt. Soc. Am. A*, 1994, **11**, 1491.



TOC: The interplay between local field enhancement and backaction determines plasmonic chiral responses and leads to widely tunable geometry-dependent optical activities.